

Modelling the Effects of Dynamic Parameters of a Self-Balancing Electric Segway over Irregular Sinusoidal Terrains

Aaron Mulumba Ntambo¹, Bernard Xavier Tchomeni kouejou¹, Desejo Filipeson Sozinando^{1*} and Alfayo Anyika Alugongo¹

¹ Vaal University of Technology, Vanderbijlpark, Department of Industrial Engineering, Operations Management and Mechanical Engineering, South Africa.

Abstract. Dynamic modelling and advanced control analysis are employed to investigate the behavior of a self-balancing electric Segway navigating on irregular sinusoidal terrains. A nonlinear dynamic model treats the Segway as a cart–inverted pendulum system, incorporating sinusoidal road irregularities and elastic and damping interactions at the wheel–ground interface. Equations of motion are derived using the Lagrangian formulation and linearized around equilibrium with Taylor expansions. Numerical simulations via the fourth-order Runge–Kutta method reveal significant increases in vibration amplitudes and system sensitivity at higher speeds. Kernel Density Estimation (KDE) is applied to translational and angular vibration data, yielding smooth distributions, while Lorenz-like attractors indicate deterministic chaos under certain excitations. Stability is assessed through bifurcation analysis, which reveals a critical forward velocity of 20.102 m/s, beyond which the system transitions into instability. The findings also identify critical thresholds, including a friction-to-mass ratio above approximately 7, a gravity-to-length ratio exceeding 25, and a mass ratio near 0.3. Each of them contributes to heightened instability and complex oscillatory responses. The significant influence of irregular terrain on system dynamics underscores the necessity for robust control strategies to maintain operational stability and rider comfort on uneven surfaces.

1 Introduction

Vehicle dynamics, tire behavior, and road profiles must be considered in explaining the dynamic vibration of Segway systems riding nonuniform sinusoidal terrains. As a self-balancing two-wheeled vehicle, Segway faces severe problems on uneven terrain, where system stability and rider comfort have much to do with each other. To overcome these issues, scholars have proposed series elastic actuators (SEA) for improving balance and reducing vibration under straight and curvilinear motion [1]. Tire–road interaction is also central in the process, particularly the ability of the tire to dissipate short-wavelength disturbances. Adhesion phenomena are accounted for by models such as the LuGre tire model and thus are essential in Segway response prediction on sinusoidal profiles [2,3].

Road roughness and cross slope raise dynamic wheel loads, which increase stresses on the vehicle and the rider's annoyance [4,5]. Roughness resistance also causes energy dissipation by vibration, and it impacts efficiency [6]. Velocity-based stabilizers have been invented to help Segways navigate dynamic terrain [7], and spring-based tire-soil interaction models allow realistic simulation of the variability of terrain [8]. Whole-body vibration (WBV), measured in terms of vibration dose values (VDV), remains a principal

indicator of safety and comfort for real-world use [9]. To mimic road irregularities realistically, high-order white noise filtering is utilized, providing realistic modelling of the system [10]. Stability in unbalanced terrain is characterized by advanced control techniques. They range from deep neural network (DNN)-compensated PD controllers [11] and discrete-time vehicle models stabilizing low-speed instability [12], to neural dynamic policies where flexibility is combined with long-term stability [13]. The influence of stochastic terrain excitations on balance control has been shown to amplify nonlinear coupling effects in self-balancing vehicles, reinforcing the need for robust stability-aware modelling approaches [14]. Other developments include discretization methodologies applied to non-minimum phase Segways [15,16], PID controllers in conjunction with deep-learning terrain perception [17], and fuzzy Kalman filters for state estimation enhancement [18]. The dynamic behaviour of a drill string under the influence of fluid forces has been analysed using nonlinear models, revealing significant impacts on vibration response and system stability [19]. Despite these advances, much remains unaddressed. Most work leaves out the combined action of nonlinear tire–ground dynamics, high-speed riding, and stable to chaotic response transitions. Few also integrate sophisticated mathematical modelling with statistics, such as kernel density estimation, to quantify probabilistic vibration behavior across regimes. This research bridges these

* Corresponding author: desejos@vut.ac.za

gaps through the development of a non-linear dynamic model of a Segway ride over sinusoidal terrain with elastic and damping at the wheel-ground interface. Based on kernel density estimation and numerical simulations, the paper reports vibration features and boundaries of criticality at which stability changes to instability, including deterministic chaos. Finally, such an integrated approach offers a novel understanding of the interactions among mechanics, road roughness, and control strategies towards enabling safer and more comfortable driving on rough roads with Segway. This article consists of the following sections: The second section describes the dynamic model of the cart-inverted pendulum system and its governing equation. The third and fourth sections present a brief overview of the simulation techniques to be used for the proposed model. In the fourth section, mathematical simulation, and the results of the third are presented. Finally, the fifth section, the conclusion and future work, is written.

2 Dynamic equation of the Segway system

The Segway dynamics may be approximated using a coupled ODE system to model its time dynamics in its state variables. They are the most important dynamics of the inverted pendulum mechanism and connect accelerations, velocities, displacements, and applied forces in the system. To make the problem mathematically tractable, some assumptions are made:

- ❖ The wheels are in contact with the ground only and roll without slip or frictional loss.
- ❖ Aerodynamic drag is not considered, assuming the non-importance of air friction.
- ❖ Mass distribution of the system is assumed to be unaltered in the analysis.
- ❖ The Segway chassis is assumed rigid without elastic deformation.
- ❖ Sinusoidal rough ground surface is modeled by a mathematical model without considering the variation of the surface material.

Fig. 1 shows the physical body of the Segway and its dynamical idealization. Fig. 1(a) illustrates the actual system, i.e., the small figure with two coaxial wheels and a vertical handlebar to provide steering and stability.

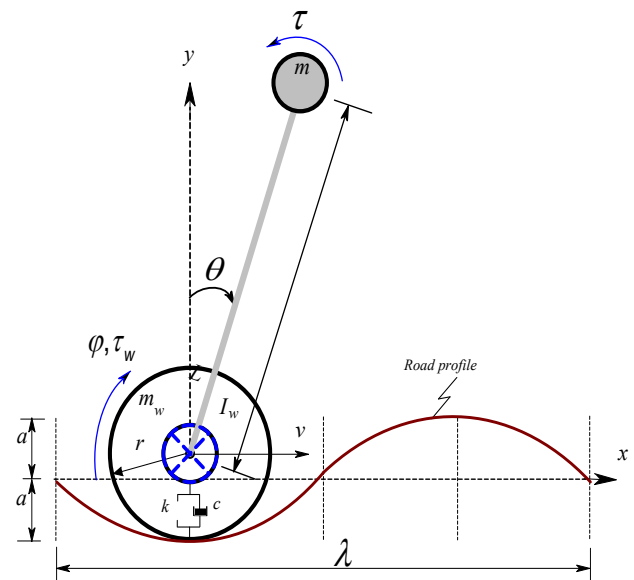


Fig.1 Physical system of electric Segway

Fig. 1(b) illustrates the system in cart-inverted pendulum configuration with three DOF, expressed by the independent coordinates x, y , and θ . This approximation maintains the inherent dynamics that control balance and motion and provides a foundation for the study of the dynamic response of the Segway in various operating regimes.

The dynamic model accounts for road irregularities by taking up the terrain as a sinusoidal profile of amplitude and wavelength λ . Wheel-ground contact is simulated by a spring-damper system having stiffness k and damping coefficient c to realize both the elastic behavior and energy dissipation that describe vibration transfer to the Segway structure. Control actions are introduced by the applied pendulum mass torque τ and wheel torque τ_w ; these are central to stability analysis. The vector position of mass m can be obtained by:

$$\begin{aligned}x_s &= x + L \sin \theta \\y_s &= y - L \cos \theta\end{aligned}\quad (1)$$

After performing algebraic manipulation based on Eq. (1), the kinetic energy can be expressed in explicit form:

$$\begin{aligned}T &= \frac{1}{2}m(\dot{x}^2 + \dot{y}^2 + 2L\dot{x}\dot{\theta} \cos \theta - 2L\dot{y}\dot{\theta} \sin \theta + 2L^2\dot{\theta}^2) \\&\quad + \frac{1}{2}m_w(\dot{x}^2 + \dot{y}^2) + \frac{1}{2}I_w\left(\frac{\dot{x}}{r}\right)^2\end{aligned}\quad (2)$$

damping in structural members, rolling resistance, and viscous behavior in joints:

$$D = \frac{1}{2}c\left(\dot{y} - \frac{2\pi av}{\lambda} \cos\left(\frac{2\pi vt}{\lambda}\right)\right)^2\quad (4)$$

The kinetic energy merges three contributions: translational movement of the cart, rotational motion of the pendulum, and rotation of the wheels. The application of Lagrange's equations of motion to derive the governing dynamics of the Segway system is based on:

$$\frac{d}{dt}\left(\frac{\partial T}{\partial \dot{q}_n}\right) - \frac{\partial T}{\partial q_n} + \frac{\partial U}{\partial q_n} + \frac{\partial D}{\partial \dot{q}_n} = \{F_q\}; \quad q_n = x, y, \theta\quad (5)$$

The 3-DOF Segway system equations of motion derived through Lagrangian mechanics (Eq. 5) are presented here in the following general form:

$$\left(m + m_w + \frac{I_w}{r^2}\right)\ddot{x} + mL\ddot{\theta} \cos \theta = \frac{\tau_w}{r}\quad (6)$$

$$(m + m_w)\ddot{y} - Lm\ddot{\theta} \sin \theta + c\left(\dot{y} - \frac{2\pi av}{\lambda} \cos\left(\frac{2\pi vt}{\lambda}\right)\right)$$

$$+ k\left(y - a \sin\left(\frac{2\pi vt}{\lambda}\right)\right) + mgL = 0\quad (7)$$

$$2mL^2\ddot{\theta} + mL\ddot{x} \cos \theta - mL(\ddot{y} + g) \sin \theta = \tau_w - \tau\quad (8)$$

The obtained mathematical model, presented through Eqs. (6) and (8) are strongly nonlinear, and analysis through the Taylor series expansion is used as:

$$f(x) = \sum_{n=0}^{\infty} \frac{1}{n!} \frac{d^n f}{dx^n}(x - x_o)\quad (9)$$

By considering small variations of x around x_o , terms of higher order and approximation, Eq. (9) can be written in a simpler linear form:

$$f(x) \approx f(x_o) + \left.\frac{df}{dx}\right|_{x=x_o} (x - x_o)\quad (10)$$

The potential energy is mainly owed to the gravitational action on the inverted pendulum and secondarily to elastic interactions with the ground.

$$U = \frac{1}{2}k\left(y - a \sin\left(\frac{2\pi vt}{\lambda}\right)\right)^2 + mgL(y - L \cos \theta)\quad (3)$$

The Rayleigh dissipation function accounts for the rate of loss of energy due to non-conservative forces,

By considering the excursions about the equilibrium position $x_o = 0$, $y_o = 0$, and $\theta_o = 0$ or π . Taylor series approximations give:

$$\begin{Bmatrix}x \\ y \\ \theta\end{Bmatrix} = \begin{Bmatrix}x_o \\ y_o \\ \theta_o\end{Bmatrix} + \begin{Bmatrix}\hat{x} \\ \hat{y} \\ \hat{\theta}\end{Bmatrix}\quad (11)$$

Therefore, the linearization relationship can be performed.

$$\begin{aligned}\sin \theta &= \sin(\theta_o + \hat{\theta}) \\&\approx \sin \theta_o|_{\theta_o=0} + \left.\frac{d}{d\hat{\theta}}(\sin \hat{\theta})\right|_{\hat{\theta}=0} (\hat{\theta} - \theta_o)|_{\theta_o=0}\end{aligned}\quad (12)$$

$$\begin{aligned}\cos \theta &= \cos(\theta_o + \hat{\theta}) \\&\approx \cos \theta_o|_{\theta_o=0} + \left.\frac{d}{d\hat{\theta}}(\cos \hat{\theta})\right|_{\hat{\theta}=0} (\hat{\theta} - \theta_o)|_{\theta_o=0}\end{aligned}\quad (13)$$

By using these expressions (12) and (13), linearized equations of motion (6), (7), and (8) can be expressed in matrix form:

$$\begin{Bmatrix}m + \frac{I_w}{r^2} & 0 & mL \\ 0 & m_w & 0 \\ mL & 0 & mL^2\end{Bmatrix} \begin{Bmatrix}\ddot{x} \\ \ddot{y} \\ \ddot{\theta}\end{Bmatrix} + \begin{Bmatrix}0 & 0 & 0 \\ 0 & c & 0 \\ 0 & 0 & 0\end{Bmatrix} \begin{Bmatrix}\dot{x} \\ \dot{y} \\ \dot{\theta}\end{Bmatrix} + \begin{Bmatrix}0 & 0 & 0 \\ 0 & k & 0 \\ 0 & 0 & -mgL\end{Bmatrix} \begin{Bmatrix}x \\ y \\ \theta\end{Bmatrix} = \begin{Bmatrix}\frac{\tau_w}{r} \\ c\dot{y} + k\dot{y} \\ \tau_w - \tau\end{Bmatrix} + \begin{Bmatrix}mL\hat{\theta}^2 \\ 0 \\ mL\hat{x}\hat{\theta}\end{Bmatrix}\quad (14)$$

The nonlinear terms $mL\hat{\theta}^2$ arise from centrifugal forces due to the rotational motion of the Segway body. It depends on the square of the angular velocity $\hat{\theta}$,

$mL\dot{x}\dot{\theta}$ which represents the Coriolis forces or coupling between the linear horizontal motion \dot{x} and the angular motion $\dot{\theta}$ of the Segway body. It is a product of two velocity terms, making it nonlinear. These nonlinear terms are essential to accurately model the dynamic behavior of the Segway system, especially during maneuvers involving changes in speed and orientation.

$$f_n = \frac{2}{L} \int_0^L f(x) \sin\left(\frac{n\pi x}{L}\right) dx \quad (15)$$

3 Brief overview of Kernel Density Estimation

Kernel Density Estimation (KDE) is used to provide a smooth, continuous estimation of the probability distribution of translational and angular vibrations in the Segway system. Its smoothed version of the histogram is utilized to provide a smooth estimate of the underlying vibration data. These are independent samples of vibration from an unknown distribution (x_1, x_2, \dots, x_n) , contributing to the density estimate.

$$\hat{\Gamma}(x) = \frac{1}{n} \sum_{i=1}^n \prod_{j=1}^d \frac{1}{h_j} K\left(\frac{x_j - x_{ij}}{h_j}\right) \quad (16)$$

$$h = \left(\frac{4\delta^5}{3n}\right). \quad (17)$$

where δ denotes the standard deviation of the vibration data, while n represents the number of collected samples.

$$K(x) = \begin{cases} 1 - |x| & \text{if } |x| < 1 \\ 0 & \text{otherwise} \end{cases} \quad (18)$$

Where the kernel function $k(x)$ is a non-negative data weight function. The smoothing parameter $h > 0$ or bandwidth parameter controls the smoothness level. Its value is determined by solving Equation (16), resulting in a scaled kernel form of the optimal-fitting vibration data.

4 Stability analysis of a self-balancing Segway Vehicle

The dynamic response of physical and engineering systems is typically modeled by differential equations that mimic how motion evolves as a function of constraint, external disturbances, and applied loads. For the Segway, nonlinear coupling between a finite number of degrees of freedom produces coupled equations of motion that are typically higher than second order. For simplicity of analysis, a Lorenz-type formulation is employed to rearrange Eqs. (6)-(8) into first-order ordinary differential equations (ODEs), in which each

state variable is expressed as a function of its time derivative and the influence of the other variables:

$$x_1 = x; y_1 = y; \theta_1 = \theta; x_2 = \dot{x}; y_2 = \dot{y}; \theta_2 = \dot{\theta}$$

$$(19) \dot{x}_1 = x_2$$

$$\dot{x}_2 = \frac{1}{m + m_w + \frac{I_w}{r^2}} \left(\frac{\tau_w}{r} - mL\theta_2 \cos \theta_1 \right) \quad (19)$$

$$\dot{y}_1 = y_2$$

$$\dot{y}_2 = \frac{1}{m + m_w} \left[mL\theta_2 \sin \theta_1 - c(y_2 - \frac{2\pi av}{\lambda} \cos(\frac{2\pi vt}{\lambda})) \right.$$

$$\left. -k(y_1 - a \sin(\frac{2\pi vt}{\lambda})) - mgL \right] \quad (20)$$

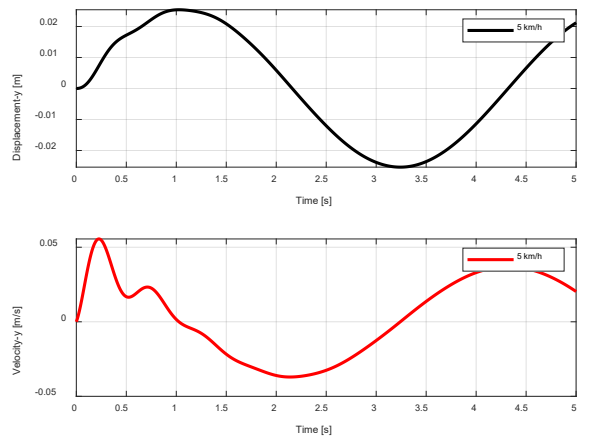
$$\dot{\theta}_1 = \theta_2$$

$$\dot{\theta}_2 = \frac{1}{2mL^2} \left[\tau_w - \tau - mL\dot{x}_2 \cos \theta_1 + mL(\dot{y}_2 - g) \sin \theta_1 \right] \quad (21)$$

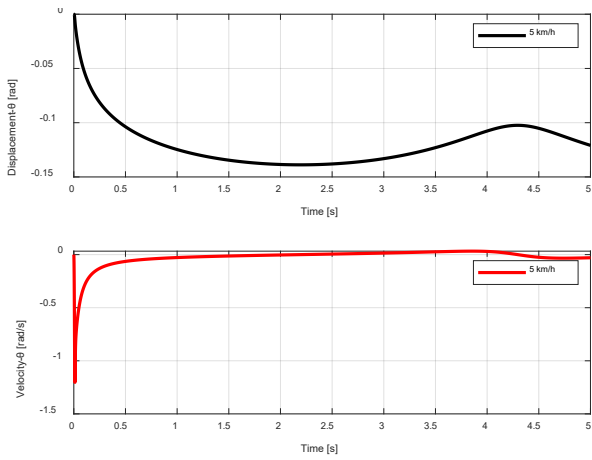
5 Numerical simulation and results

The numerical simulation of the Segway system employs specific physical and mechanical parameters characterizing the vehicle's dynamics. The mass of the Segway body is taken as 1.2 kg, while each wheel possesses a mass of 0.2 kg. The moment of inertia of the wheel about its rotation axis is $0.02 \times 10^{-3} \text{ kgm}^2$, reflecting the wheel's resistance to angular acceleration. The distance from the Segway's center of mass to the axis of rotation, denoted as L , is set to 0.075 m. The radius of the wheel r is 0.032 m. The stiffness coefficient k that represents the elastic restoring force is 0.29 N/m. Additionally, damping effects, accounting for the energy dissipated due to motion, are modelled by a damping coefficient $c = 0.01 \text{ Ns/m}$. The wavelength of the sinusoidal road profile λ over which the Segway operates is defined as 6 m.

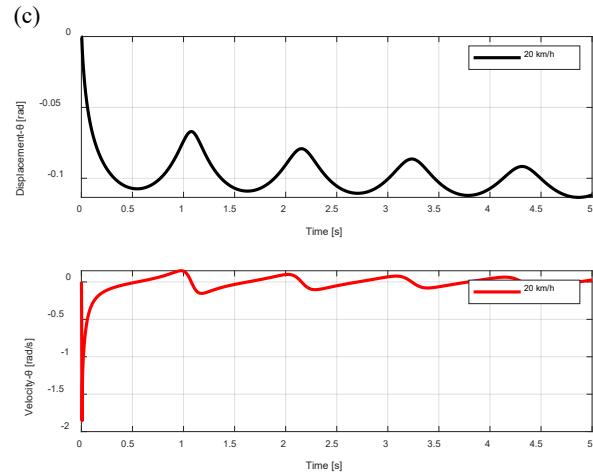
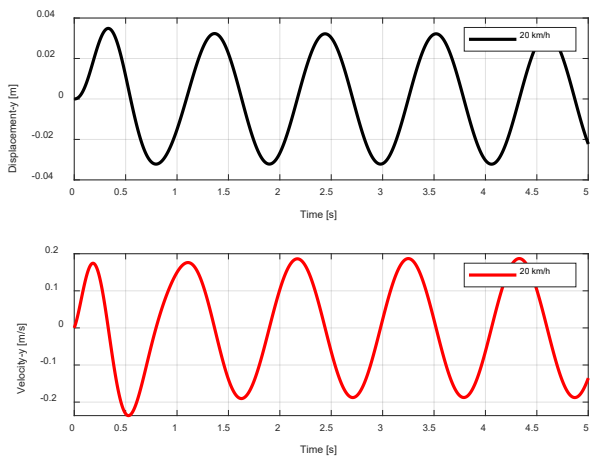
The Runge-Kutta 4th order was employed as a discretization method for the vibration response of the Segway system generated under a specific irregular road profile. Meaning that the signal's step size may be large so that the output is more widely spaced, and the interpolant is called up to produce more finely spaced results. The results of the dynamic analysis of the Segway system on an irregular sinusoidal road profile are processed using MATLAB program. The obtained signal considers the vibrations generated by all the constituent assembly elements of the Segway system, is presented in a Waveform and a KDE histogram.



(a)



(b)



(d)

Fig. 2. Displacement and velocity time response (a) y-coordinate at 5 km/h; (b) θ -coordinate at 5 km/h; (c) y-coordinate at 20 km/h; (d) θ -coordinate at 20 km/h.

The y-coordinate displacement in Figure 2(a) exhibits a low oscillatory behavior with a smooth amplitude not exceeding approximately ± 0.025 m. The waveform indicates that the suspension and damping mechanisms effectively mitigate road-induced excitations at 5 km/h. Correspondingly, the y-velocity demonstrates a relatively gentle variation, peaking near ± 0.05 m/s. The characteristics suggest that the system operates under a regime where inertial forces remain minor, and road irregularities are primarily absorbed through elastic and damping elements, maintaining the system near stable equilibrium. The angular displacement θ in Figure 2(b) reveals a slow convergence from an initial offset of nearly -0.15 rad toward a less pronounced oscillatory state. The decrease in amplitude indicates effective stabilization due to the restoring torque and control mechanisms inherent to the inverted pendulum dynamics. Angular velocity exhibits a rapid initial transient before settling into smaller oscillations by confirming the presence of a damping effect that limits large angular displacements. When the Segway operates at 20 km/h, a marked increase in dynamic activity is evident. Figure 2(c) shows the y-coordinate displacement presenting higher oscillations with a peak amplitude approaching ± 0.04 m. The response reveals increased system sensitivity to road irregularities at elevated speeds, where kinetic energy inputs amplify the magnitude and vibrations transmitted through the suspension. The y-velocity also demonstrates significant fluctuations, rising to approximately ± 0.2 m/s. The larger velocity variation indicates a dynamic regime with the influence of growth in inertial effects, and the response transitions toward conditions where potential resonance with road excitation might occur. Figure 2(d) illustrates the θ -coordinate response, displaying sustained oscillations rather than the smooth decay observed at 5 km/h. Angular displacement at 20 km/h oscillates with a higher frequency and a peak amplitude slightly exceeding 0.1 rad, indicating an increase in forward velocity leading to stronger coupling between the translational motion and pendulum dynamics. The corresponding angular velocity shows fluctuations

arising from the non-linear interactions between the inverted pendulum's gravitational restoring moments and the inertial forces imposed by the higher travelling speed.

Further, in Figure 3, Kernel density estimation (KDE) applied to time-domain vibration signals provides a probability distribution of amplitudes or extracted features, from which fault-related information can be derived by analyzing their statistical characteristics.

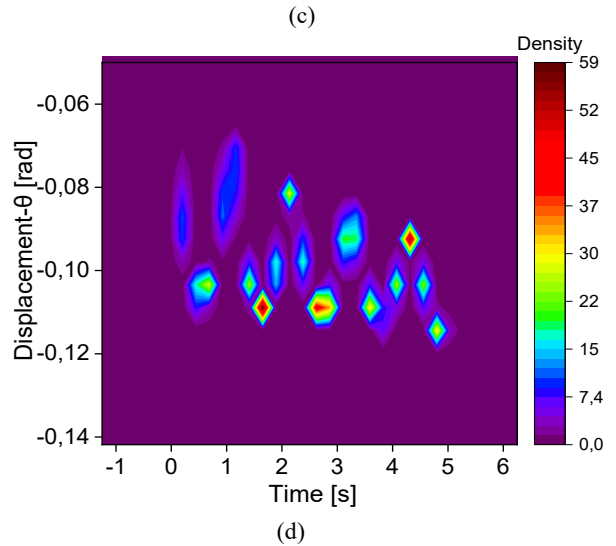
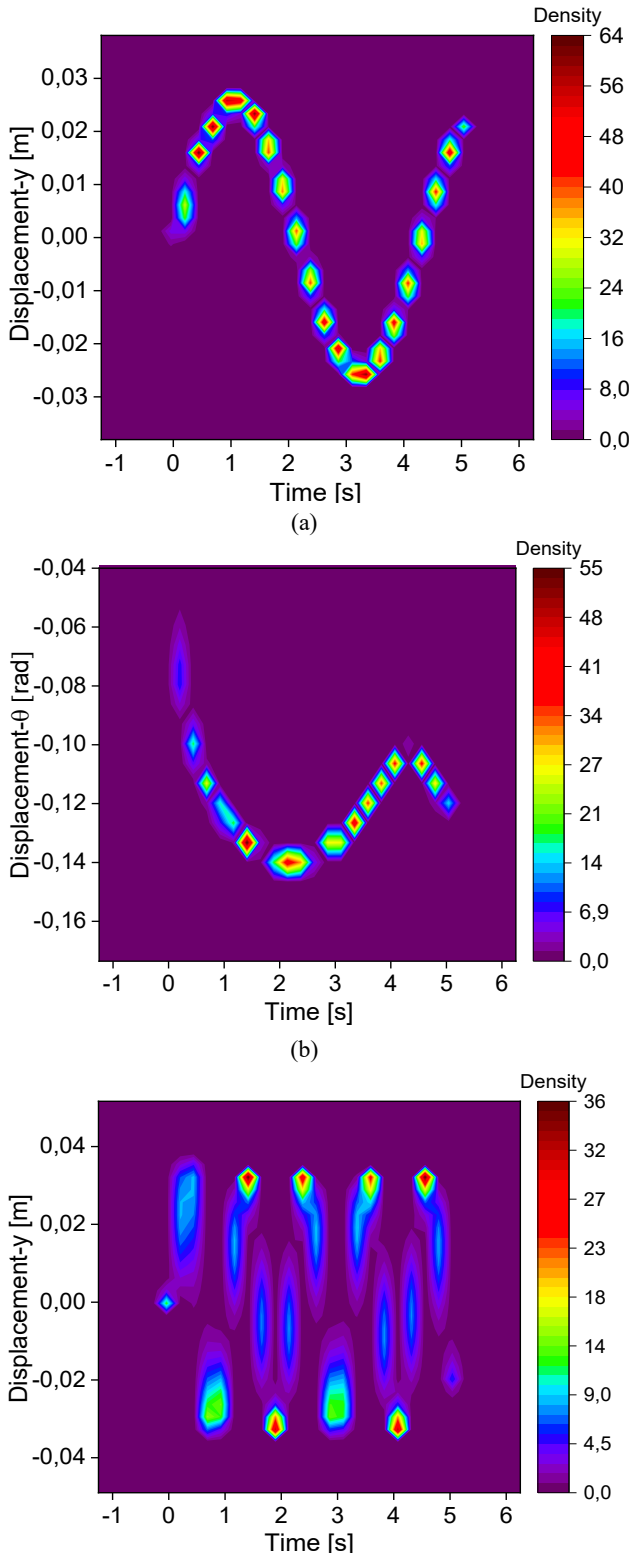


Fig. 3. KDE Spectrum response: (a) y-coordinate at 5 km/h; (b) θ -coordinate at 10 km/h; (c) y-coordinate at 15 km/h; (d) θ -coordinate at 20 km/h.

The KDE spectrum in Figure 3(a) exhibits a well-defined, smooth sinusoidal pattern in displacement along the y-axis, with the highest density regions shown in yellow and red hues closely following the trajectory of the periodic oscillation. The narrow density bands indicate low variability in the displacement data, indicating that at 5 km/h, the system maintains highly consistent translational motion. The confinement of density contours confirms that vibratory deviations remain minimal, and the system operates within a predictable dynamic range. Figure 3(b) presents the density distribution for angular displacement θ at 10 km/h. The KDE contours display an initial sharp displacement near -0.16 rad, gradually approaching a less negative value around -0.04 rad over time. Density remains concentrated in specific regions, indicating that the majority of θ -displacement samples cluster around certain trajectories rather than dispersing widely. The gradual convergence of density regions indicates that while angular motion experiences transient disturbances, the system's dynamics tend toward stabilization under moderate speeds. The KDE response in Figure 3(c) reveals a significantly more complex pattern for the y-coordinate displacement at 15 km/h. Multiple density peaks and valleys appear throughout the time, forming a series of distinct lobes in the KDE plot. This fragmented density structure indicates heightened variability and the presence of higher-frequency components superimposed on the base oscillatory motion. The increased spread in density contours signals that at 15 km/h, the Segway system encounters more pronounced dynamic excitations, resulting in less predictable translational displacement behavior. Figure 3(d) depicts the angular displacement θ at 20 km/h and shows a highly scattered density landscape. Multiple distinct density clusters are visible, dispersed across varying displacement levels between approximately -0.12 rad and -0.04 rad. Unlike the smooth convergence seen at lower speeds, the angular displacement at 20 km/h displays significant variability, with density peaks indicating intermittent, localized angular excursions. The spread and multiplicity of density regions indicate that at elevated speeds, the angular dynamics of the inverted pendulum become more sensitive to road-induced excitations and inertial forces, leading to complex oscillatory behavior.

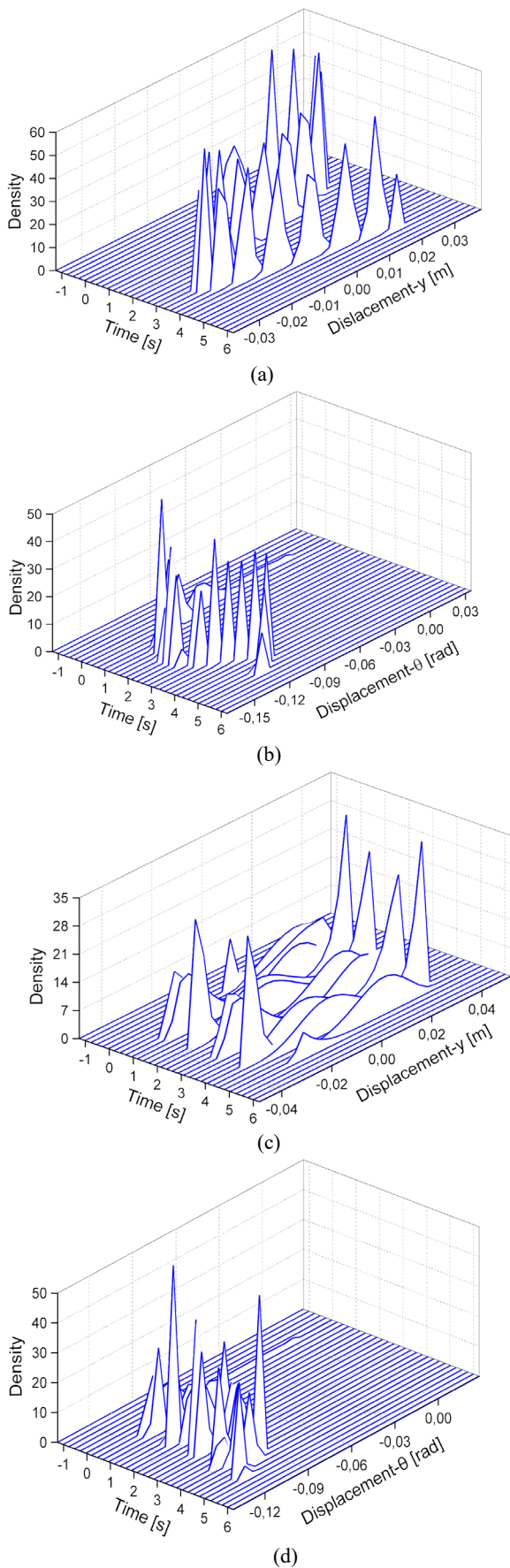


Fig. 4. KDE 3D waterfall response: (a) y-coordinate at 5 km/h; (b) θ -coordinate at 10 km/h; (c) y-coordinate at 15 km/h; (d) θ -coordinate at 20 km/h.

Figure 4(a) illustrates the KDE waterfall response for the y-coordinate displacement at a forward velocity of 5 km/h. The surface displays sharp and well-defined peaks concentrated around a smooth, sinusoidal oscillatory path. Density values reach approximately 50, reflecting the dominance of specific displacement values over time. The peaks are consistently spaced with similar magnitudes, indicating a regular, low oscillation with minimal variation. The behavior confirms that at 5 km/h, the translational dynamics remain stable and exhibit low variability responses closely following the sinusoidal excitation induced by the road profile. Figure 4(b) presents the angular displacement θ at 10 km/h. The density surface shows fewer but distinct peaks aligned along a trajectory that reflects a gradual transition from larger negative angular displacements toward smaller magnitudes. Density values peak around 40, indicating significant probability concentration at specific angular positions. The waterfall pattern indicates a rapid initial response followed by a gradual settling trend. The absence of widespread density dispersion signifies that the system retains a relatively controlled angular response under moderate speeds, although with noticeable transient effects compared to the smoother behavior at 5 km/h. The plot in Figure 4(c) for the y-coordinate displacement at 15 km/h reveals a considerably more complex density surface. Peaks appear more numerous, irregular, and distributed across a broader displacement range, extending between approximately -0.04 m and 0.04 m. The density maxima are lower, reaching around 28, which reflects increased variability in the data. The presence of multiple undulating ridges and troughs indicates higher-frequency components and intermittent bursts of elevated displacement, suggesting that the Segway's translational dynamics become more chaotic and less predictable. Figure 4(d) displays the angular displacement θ at 20 km/h, revealing a highly fragmented density surface with multiple sharp peaks dispersed over time and displacement magnitude. Density values remain relatively high, reaching about 40, but the peaks are narrower and more irregularly spaced compared to lower speeds. The pattern indicates significant fluctuations and abrupt changes in angular displacement, consistent with stronger nonlinear dynamic interactions at elevated speeds.

After presenting the KDE-based 3D cascade response, the stability of the Segway model is further analyzed via a Lorenz-type system representation (Figure 5), where bifurcation analysis is used to reveal the nonlinear dynamic behavior of the system (Figure 6).

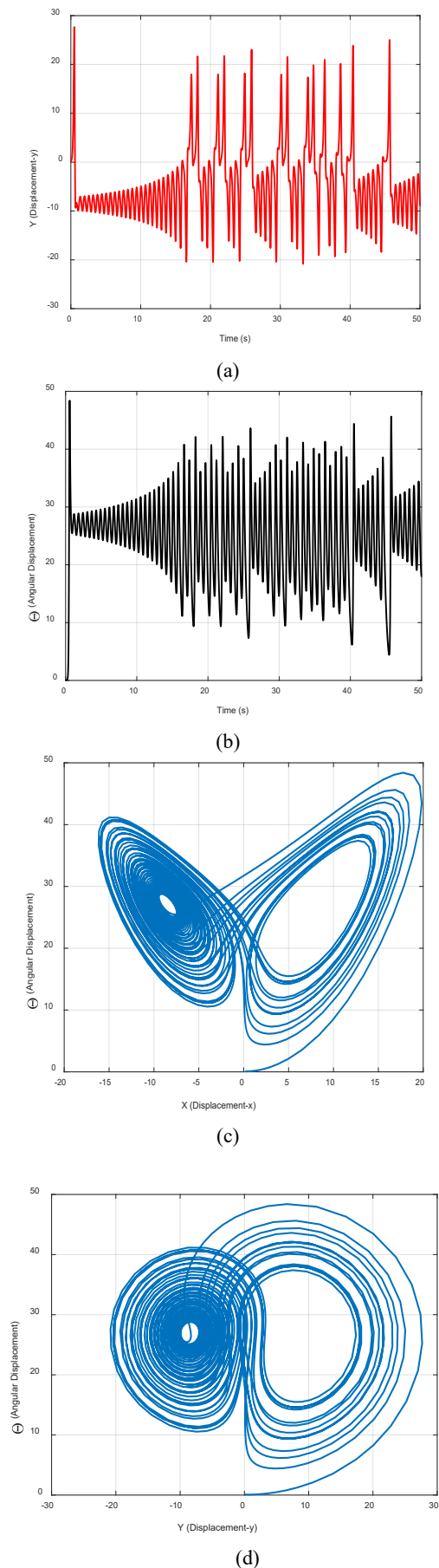


Fig. 5. Lorenz-like system: (a) y-coordinate response; (b) θ -coordinate response; (c) θx attractor; (d) θy attractor.

Figure 5(a) presents the time history of the y-coordinate displacement over a period of 50 s. The waveform exhibits non-stationary oscillations with clear amplitude modulation, with initial oscillations displaying smaller amplitudes and remaining relatively regular. Over time, the oscillation amplitudes increase and the pattern grows more irregular, which indicates greater system excitation and the effects of nonlinear interactions. Peaks and troughs vary significantly in magnitude and frequency, indicating the system is experiencing complex dynamic states rather than quasi-periodic motion. Figure 5(b) depicts the time response of angular displacement θ over the same period with a similar trend to the y-coordinate but with more pronounced high oscillations. The early segments of the response show damped oscillations with moderate amplitude that gradually shift into larger and more erratic fluctuations as time progresses. The growth in oscillation amplitude and complexity points to the strong influence of nonlinear coupling between translational and angular motions, reflecting the inherent instability of the inverted pendulum dynamics under certain excitation conditions. Figure 5(c) visualizes the state-space attractor formed by plotting angular displacement θ against x-coordinate displacement. The resulting trajectory resembles the classical Lorenz attractor and shows a pair of lobes connected by swirling paths. The structure indicates deterministic chaos where trajectories evolve around two unstable equilibrium regions and shift between them over time. The dense looping paths signify that small differences in initial conditions can lead to significantly divergent system states over time, confirming the presence of sensitive dependence on initial conditions. Figure 5(d) displays the attractor generated by plotting θ against the y-coordinate displacement. The pattern retains the distinctive double-lobed shape with tightly wound loops inside each lobe. In comparison to Figure 6(c), the attractor in Figure 5(d) appears slightly more concentrated and indicates that although chaos remains present, the coupling between θ and y may be somewhat less dispersive than the coupling between θ and x. Still, the trajectory displays a similar dynamic signature where oscillations shift unpredictably between the lobes and highlight the inherently unstable nature of the Segway system under certain dynamic regimes. The emergence of Lorenz-like attractors, bifurcation patterns, and transitions from stable to chaotic regimes observed are consistent with nonlinear Segway models operating under irregular terrain excitation and parameter variation [14]. The bifurcation control parameters are defined by the influence of damping, gravitational effects, and mass distribution on system stability. Each parameter provides how mechanical properties and physical forces govern the conditions under which the Segway may transition between stable and unstable dynamic states. The dimensionless forms that characterize the parameters governing the dynamic behavior of the Segway system are summarized in Table 1.

Table 1. Bifurcation control parameters and associated physical quantities

Parameter	Definition	Physical Meaning
Friction/Mass ratio	$\sigma = c/m + m_w$	Damping strength
Mass ratio	$\beta = m/m + m_w$	Mass coupling between the cart and pendulum
Gravity/Length ratio	$\rho = g/L$	Gravity-driven restoring force

Figure 6(a) shows how the maximum angular displacement z varies with σ . At small values of σ (less than ~ 2), the system has small, stable oscillations, because small disturbances are damped out by friction.

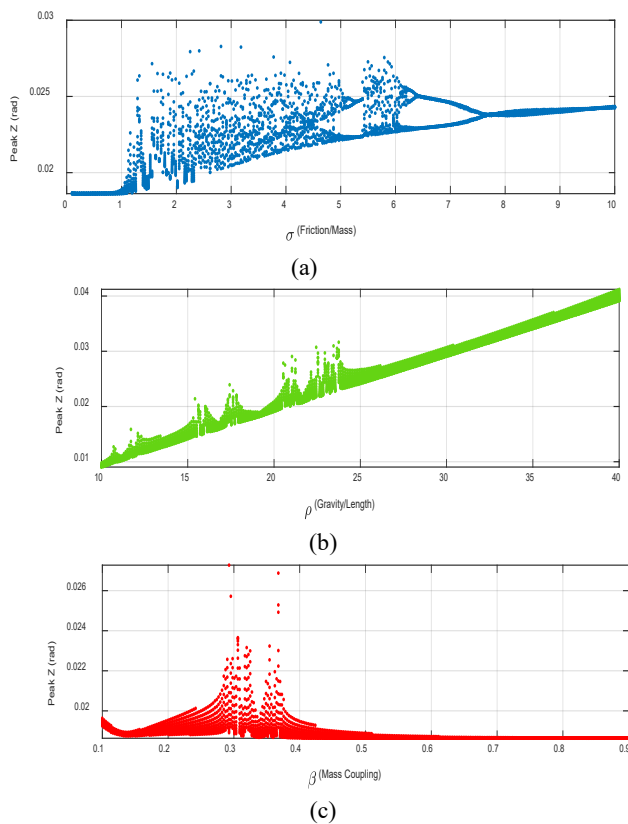


Fig. 6. Bifurcation diagram of coupling effects: (a) σ ; (b) ρ , and (c) β on the Segway dynamic system.

Figure 6(a) displays peak angular displacement Z as a function of σ . At low values of σ below approximately 2, the system exhibits low-amplitude oscillations and reveals stable dynamics where small perturbations become damped by frictional forces. When σ increases beyond the range, the bifurcation diagram reveals a spread of data points and branching patterns that signify the onset of more complex oscillatory behaviors. The appearance of bifurcation branches around $\sigma \approx 4$ to $\sigma \approx 6$ indicates an increase in the friction-to-mass ratio by introducing nonlinear effects that destabilize the system, leading to oscillations of varying amplitude. Beyond $\sigma \approx 7$, the oscillations gradually stabilize again, reflected in the convergence of peak Z values to a narrow band, indicating the re-emergence of more predictable

dynamics at high damping levels. Figure 6(b) shows the relationship between Z and the gravity-to-length ratio ρ . Across the range studied, peak Z values display an increasing trend as ρ grows and reflect stronger gravitational restoring forces acting on the pendulum. Between approximately ρ of 15 and 25, the response reveals oscillatory fluctuations in peak Z with intermittent clusters of higher values. The fluctuations demonstrate that certain ranges of gravitational stiffness may induce parametric resonances. Above $\rho \approx 25$, the growth of Z appears smoother, showing a dominant stabilizing effect of gravity for large ρ . However, the persistence of minor fluctuations implies that even strong gravitational restoring forces cannot completely suppress dynamic irregularities under certain conditions. Figure 6(c) illustrates how peak Z varies with the mass ratio β . The diagram shows a pronounced bifurcation structure centered around $\beta \approx 0.3$, where the peak displacement amplitude spreads over a wide range. The spread indicates significant sensitivity of the system's dynamics to the proportion of mass between the pendulum and the wheel assembly. Near this critical mass ratio, the dynamic coupling between translational and rotational motion appears strongest, promoting the emergence of large amplitude oscillations and complex dynamic states. For values of β outside the range of approximately 0.25 to 0.4, peak Z values diminish sharply, and the bifurcation structure collapses into a narrow band, indicating stable system behavior with low amplitude oscillations.

6 Conclusion

This study developed a nonlinear dynamic model to describe the dynamics of a self-balancing electric Segway moving on wavy sinusoidal surfaces. The model included wheel-ground damping and elasticity and, by using Lagrangian mechanics, derived the system's governing equations. Fourth-order Runge-Kutta scheme simulations showed that higher forward velocities enhance vibrations and can propel the Segway from stable motion towards chaos, which is depicted in Lorenz-like state-space plots. Probabilistic distributions of angular and translational vibrations were studied through kernel density estimation. The stability boundaries were determined through bifurcation plots, and a speed of about 20.1 m/s at which it loses stability was determined. The study also examined the effect of parameters like friction-to-mass ratio, gravity-to-length ratio, and mass distribution on oscillatory behavior and determined ranges of parameters for which vibration is more vigorous. These results constitute the foundation of control methods for terrain-exciting forces and nonlinear couplings, achieving stable motion and attenuating complex oscillations. Future research may be further extended to human-vehicle interaction phenomena, experiments, and adaptive control methods-possibly machine learning based-against nonlinearities on various terrains and velocities.

Nomenclature

Symbol	Description	Units
x	Horizontal displacement of the Segway cart	m
y	Vertical displacement of the Segway cart	m
θ	Angular displacement of the inverted pendulum	rad
\dot{x}	Horizontal velocity of the Segway cart	m/s
\dot{y}	Vertical velocity of the Segway cart	m/s
$\dot{\theta}$	Angular velocity of the inverted pendulum	rad/s
m	Mass of Segway body (pendulum)	kg
m_w	Mass of one wheel	kg
I_w	Moment of inertia of wheel about its axis	kg·m ²
L	Distance from Segway center of mass to axis of rotation	m
r	Radius of wheel	m
k	Spring stiffness coefficient of wheel-ground interaction	N/m
c	Damping coefficient of wheel-ground interaction	Ns/m
a	Amplitude of sinusoidal road profile	m
λ	Wavelength of sinusoidal road profile	m
τ	Torque applied to pendulum mass	N·m
τ_w	Torque acting on wheels	N·m
T	Kinetic energy of the Segway system	J

U	Potential energy of the Segway system	J
D	Rayleigh dissipation function	J/s
F_q	Generalized external force vector	N or N·m
ω	Angular frequency	rad/s
φ	Angular displacement of the wheel	rad
f	Frequency	Hz
h	Bandwidth in kernel density estimation	–
$K(\cdot)$	Kernel function	–
h	Bandwidth matrix in multivariate KDE	–
n, d	Number of data samples	–
Z	Peak angular displacement	rad
t	Time	s

References

1. H. Yun, H. Zhang, J. Lee, Stability Improvement of Segway Based on Tire Model Using the SEA. *Robotica* 39, 42-54 (2021).
2. F. Alobaid, S. Taheri, The Modified In-Plane Rigid-Elastic-Coupled Tire Modal Model: Dynamic Response to Short Wavelength Road Profiles. *Vehicle System Dynamics* 62, 3076-3097 (2024).
3. J. Zhang, S. Yang, S. Li, Y. Lu, H. Ding, Influence of vehicle-road coupled vibration on tire adhesion based on nonlinear foundation. *Applied Mathematics and Mechanics* 42, 607–624 (2021).
4. K. Srikanth, V. Chowdary, Influence of roughness and cross slope induced dynamic loads on flexible pavement responses. *International Journal of Pavement Engineering* 24, 2241101 (2023).
5. S. Kakara, V. Chowdary, Effect of pavement roughness and transverse slope on the magnitude of wheel loads. *Arabian Journal for Science and Engineering* 45, 4405–4418 (2020).
6. M.M. Turner, Cycling on rough roads: a model for resistance and vibration. *Vehicle System Dynamics* 62, 2729–2749 (2024).
7. S.A. Kumar, B. Sharma, J. Vanualailai, A. Prasad, R. Chand, New players in intelligent transportation: autonomous Segway in a dynamic environment. *Engineering Applications of Artificial Intelligence* 126, 107107 (2023).
8. E. Koutras, F. Moretti Leila, A. Ribaric, S. Natsiavas, A new contact and road model for multi-

- body dynamic simulation of wheeled vehicles on soft-soil terrain. *Multibody System Dynamics* 63, 39–62 (2025).
9. U. Kirbaş, Effects of pothole type pavement distress on whole-body vibration. *Road Materials and Pavement Design* 24, 1403–1424 (2023).
 10. S.A. Chen, X.W. Li, J.C. Wang, High-order filtering white noises modulated by coherent and incoherent functions based road irregularities. *IEEE Transactions on Intelligent Vehicles* 9, 3952–3963 (2024).
 11. T. Zhaojia, H. Yu, W. Ping, Using DNN-compensator coupling PD-controller strategy control two-wheeled robots upright motion balance. *Journal of Field Robotics* (2024).
 12. G. Zhan, Q. Ge, H. Gao, Y. Yin, B. Zhao, S. Eben Li, An explicit discrete-time dynamic vehicle model with assured numerical stability. *Vehicle System Dynamics*, 1–24 (2024).
 13. D. Totsila, K. Chatzilygeroudis, V. Modugno, D. Hadjivelichkov, D. Kanoulas, Sensorimotor learning with stability guarantees via autonomous neural dynamic policies. *IEEE Robotics and Automation Letters* (2025).
 14. D.F. Sozinando, B.X. Tchomeni, A.A. Alugongo, Modelling dynamic parameter effects in designing robust stability control systems for self-balancing electric Segway on irregular stochastic terrains. *Physics* 7, 46 (2025).
 15. Y. Wang, G. Zhu, Performance improvement of an NMP Mini Segway using sample and hold inputs. *Applied Sciences* 13, 1070 (2023).
 16. Y. Wang, G.G. Zhu, R. Mukherjee, Performance improvement demonstration of an NMP system using sample and hold inputs. *International Journal of Dynamics and Control* 9, 109–120 (2021).
 17. C. Yan, X. Li, Research on stability control system of two-wheel heavy-load self-balancing vehicles in complex terrain. *Applied Sciences* 14, 7682 (2024).
 18. Y. Ma, F. Meng, S. Xiong, Design and implementation of a two-wheeled self-balancing car using a fuzzy Kalman filter. *Applied Sciences* 14, 5296 (2024).
 19. B.X. Tchomeni Kouejou, D.F. Sozinando, A.A. Alugongo, Modeling and Analysis of Drill String–Casing Collision under the Influence of Inviscid Fluid Forces. *Applied Sciences* 13, 3557 (2023).